Pergamon

Ultrasound in Med. & Biol., Vol. 21, No. 7, pp. 871–883, 1995

0301-5629/95 $9.50 + .00

0301-5629(94)00146-4

●*Original Contribution*

ELASTICITY IMAGING FOR EARLY DETECTION OF RENAL PATHOLOGY

S. Y. EMELIANOV,[†‡] M. A. LUBINSKI,[†] W. F. WEITZEL,[*] R. C. WIGGINS,[*] A. R. SKOVORODA[‡] and M. O'DONNELL[†]

[†]Electrical Engineering and Computer Science Department and Bioengineering Program, and [*]Division of Nephrology, Department of Internal Medicine, University of Michigan, Ann Arbor, MI, USA; [‡]Institute of Mathematical Problems of Biology, Russian Academy of Sciences, Pushchino, Russia

(*Received* 30 *June* 1994; *in final form* 3 *October* 1994)

Abstract—Early detection of renal pathology may be possible with elasticity imaging. This hypothesis was experimentally tested by quantitatively imaging internal mechanical strain due to surface deformations in an *in vitro* animal model of nephritis. Preliminary data support the hypothesis that kidney elasticity changes with renal damage and concomitant scarring before problems are detectable by traditional diagnostic techniques such as laboratory measurements of renal function.

Key Words: **Elasticity imaging, Strain imaging, Young's elastic modulus, Ultrasound, Kidney, Rabbit model of anti-GBM disease, Renal pathology, Scarring, Renal fibrosis.**

INTRODUCTION

Soft tissue elasticity can change markedly with pathology, especially in those processes including either edema or scarring. Because of this, simple palpation remains a leading diagnostic procedure for many diseases near the body surface, such as breast and testicular cancer. Recently, elasticity imaging has been proposed to evaluate the elastic properties of internal soft tissue structures inaccessible to palpation. Using deformations applied at the body surface, internal displacement and strain fields within deep lying structures have been imaged (Dickinson and Hill 1982; Eisensher et al. 1983; Tristam et al. 1986, 1988; Krouskop et al. 1987; Lerner and Parker 1987; Lerner et al. 1988, 1990; Meunier and Bertrand 1989; Axel and Dougherty 1988; Zerhouni et al. 1988; Adler et al. 1989, 1990; Bertrand et al. 1989; Parker et al. 1990; Yamakoshi et al. 1990; Yamashita and Kubota 1990; Ishihara et al. 1990; Sarvazyan and Skovoroda 1990, 1991; Ophir et al. 1991; O'Donnell et al. 1991, 1993, 1994; Lee et al. 1991; Parker and Lerner 1992; Ponnekanti et al. 1992; Ryan et al. 1992; Yemelyanov et al. 1992; Fowlkes et al. 1992; Chen et al. 1992; Skovoroda et al. 1994; Emelianov et al. 1995).

The elastic properties of any continuous medium such as tissue can be assessed by precisely measuring mechanical deformations throughout that medium induced by forces applied at the surface. Using modern medical imaging devices to measure internal motion, the elastic properties of internal organs can be estimated and even imaged (O'Donnell et al. 1993, 1994; Skovoroda et al. 1994; Emelianov et al. 1995). Although conventional imaging systems are used for internal motion tracking, elasticity imaging represents a *new* modality where the primary contrast mechanism is the Young's (or shear) elastic modulus of soft tissue. Consequently, choosing a conventional imaging system for elasticity measurements is based on its ability to track internal motion, not on overall image quality. Compared to other systems, ultrasound has two major advantages: first, it is inherently real time; and second, speckle artifacts limiting conventional image quality provide excellent markers for accurately tracking tissue motion. It has the additional benefits of being relatively inexpensive and noninvasive.

In earlier studies we showed that ultrasound speckle tracking methods can be extended, permitting measurements of internal displacement and strain fields over a wide dynamic range of tissue motion

Address correspondence to: S. Y. Emelianov, Electrical Engineering and Computer Science Department and Bioengineering Program, University of Michigan, 2350 Hayward 3304 G. G. Brown, Ann Arbor, MI 48109. E-mail: emelian@eecs.umich.edu

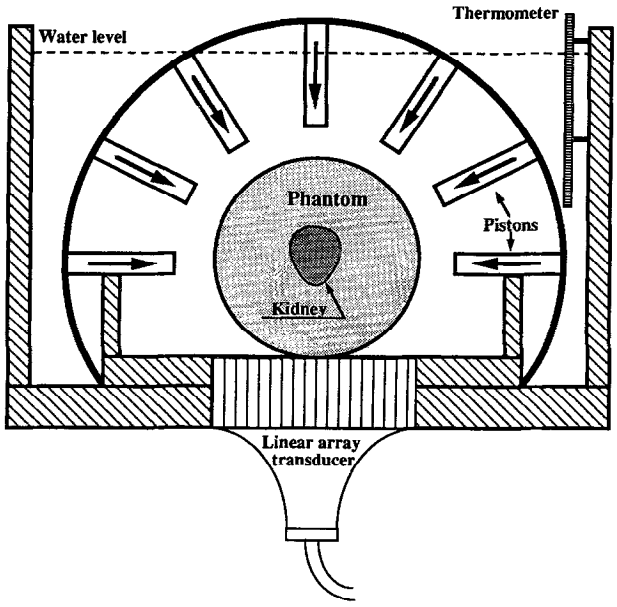

Fig. 1. Schematic two-dimensional representation of the experimental system and phantom geometry. The cylindrical phantom with a kidney at the center is 88 mm in diameter and 140 mm long. At the bottom it contacts a 128-element linear transducer array used to image the central cross-sectional plane. A set of hydraulically driven pistons deforms the top of the phantom, where only the central piston was used in the present experiments.

(O'Donnell et al. 1994). We have also compared these measurements with theoretical predictions of internal displacement and strain based on a linear elastic model, showing reasonable resolution and accuracy (Skovoroda et al. 1994). Experiments reported in previous articles were performed on gel-based tissue mimicking phantoms. In this article, we explore the applications of these methods to renal pathology.

In the kidney two types of pathology may be detected and quantified by elasticity imaging. First, there may be localized changes in elasticity produced by neoplasm, infection, embolism and/or infarction. Second, elasticity measurements may help to detect diseases at an early stage which diffusely affect the kidney. This latter group represents an important clinical problem because current noninvasive laboratory and imaging methods are insensitive and nonspecific in detecting either inflammatory renal disease or interstitial fibrosis. In the native kidney, for example, 25% to 30% nephron loss must occur before either serum creatinine or glomerular filtration rate change significantly (Harris et al. 1986). In the transplanted kidney, chronic progressive fibrosis ("chronic rejection") is a common problem in most recipients whose allografts survive through the immediate posttransplant period (Dunnill 1988) and accounts for the largest proportion of graft losses after the first 3 months (Chapman and Allen 1988). Because of significant risk and cost, frequent biopsy to detect progressive fibrosis is not feasible. Thus, extensive irreparable damage frequently occurs before biopsy and therapeutic interventions take place. A safe means of assessing renal fibrosis and distinguishing fibrotic changes and acute/edematous processes from normal is needed.

In this study we present preliminary results on animal studies testing the hypothesis that elasticity imaging can detect renal scarring which diffusely affects kidney parenchyma. A well-established rabbit model of anti-GBM glomerulonephritis which can create disease states in kidneys with varying degrees of scarring and inflammation (Downer et al. 1988) is described in the Methods and Materials section. This model closely reproduces the problems arising in clinical kidney disease. Also described in this section is an ultrasonic method to precisely measure internal tissue displacement and strain produced by an externally applied force (O'Donnell et al. 1994; Skovoroda et al. 1994). Results of some initial *in vitro* measurements are presented in the next section. We conclude with a discussion of the results.

METHODS AND MATERIALS

In the present study, three issues were addressed. First, the large strain method developed previously (O'Donnell et al. 1994) was tested for imaging highly inhomogeneous organs such as the kidney. Then, control studies were performed to validate the experimental protocol developed for elasticity imaging of both normal and diseased kidneys. Finally, experiments using kidneys excised from rabbits with experimental anti-GBM antibody disease were performed *in vitro* to test the potential diagnostic value of elasticity imaging. Details of these experiments are given below.

Initial kidney studies with a goat model

As a preliminary test of elasticity imaging in a highly inhomogeneous organ such as the kidney, a simple study was performed on excised goat kidneys. Goat kidneys closely approximating the size of human ones were chosen for these initial tissue experiments. Kidneys were obtained from a goat following an acute surgical experimental procedure during which full anesthesia was maintained. Both kidneys were removed immediately after sacrifice. One kidney was injected at two sites with 2 mL of 2% glutyraldehyde at each pole to cause crosslinking and a stiffer, "hard" region. Although artificial, this procedure produces a significant increase in tissue elasticity in specific regions testing the ability of the experimental methods to differentiate these changes.

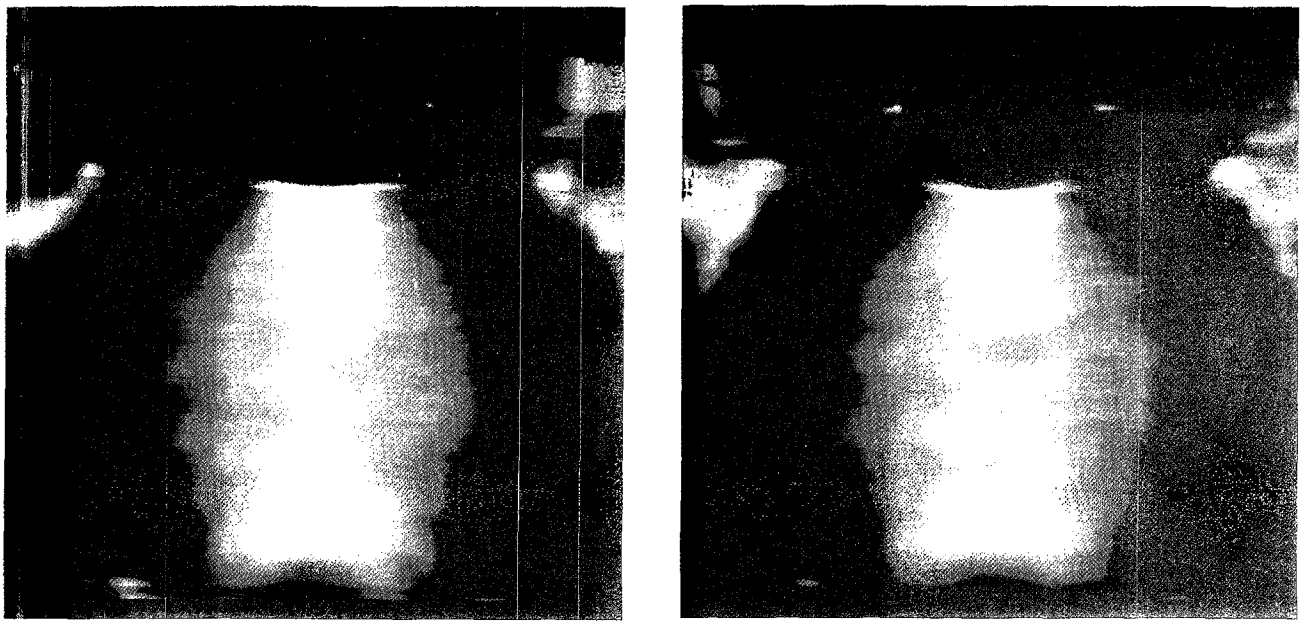

Fig. 2. Images (100 mm by 100 mm) of the vertical, longitudinal component (ϵ_{22}) of the strain tensor for the (A) homogeneous phantom and (B) composite homogeneous phantom with backfilled hole in the center.

Rabbit model of nephritis

Experiments using kidneys excised from rabbits with experimental anti-GBM antibody disease were performed *in vitro* to mimic the clinical environment for normal and transplanted kidneys. Two major types of injury are well modeled in the rabbit with this disease. At day 7 after anti-GBM antibody injection, proteinaceous crescents are present in Bowman's space

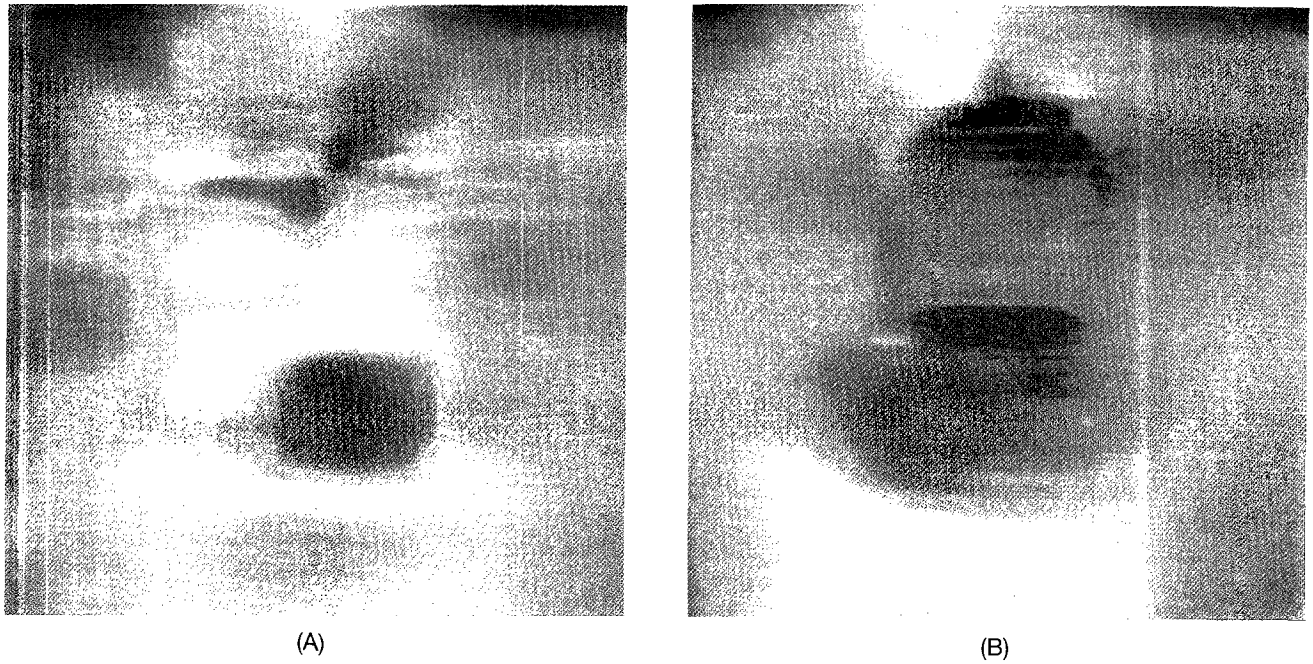

Fig. 3. Magnified (50 mm by 50 mm) images of the vertical, longitudinal component (ϵ_{22}) of the strain tensor for the central part of the phantom: (A) normal goat kidney and (B) goat kidney with glutyraldehyde "inclusions."

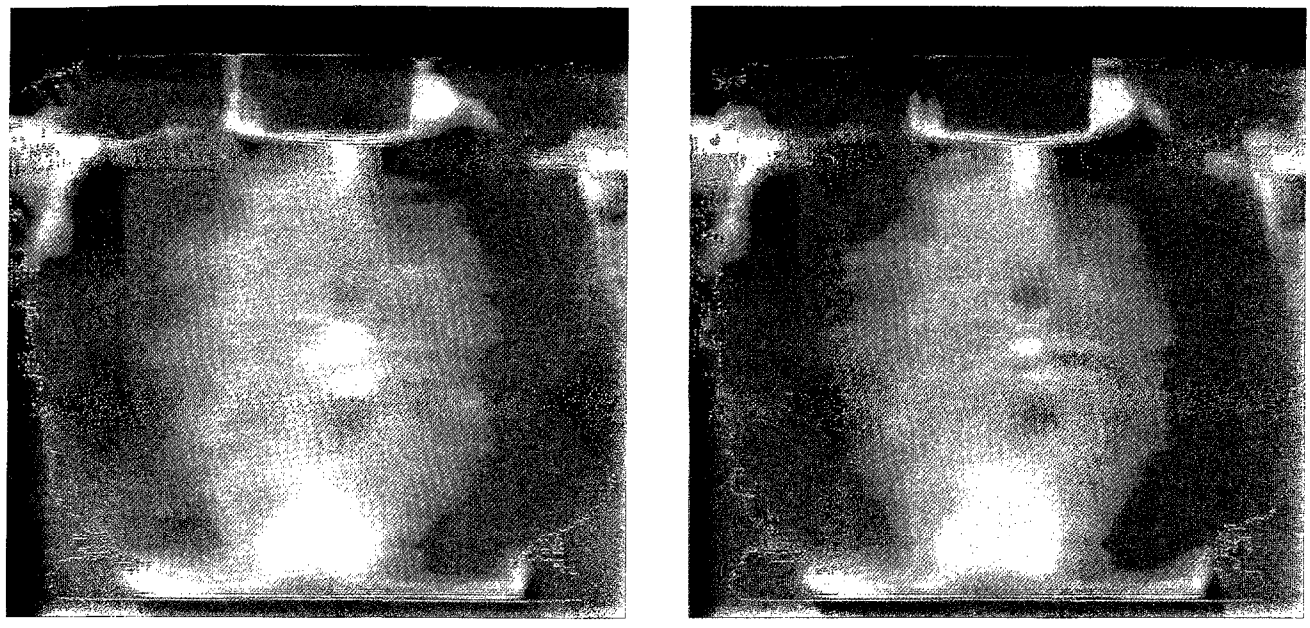

Fig. 4. Images (100 mm by 100 mm) of the vertical, longitudinal component (ϵ_{22}) of the strain tensor for the phantom with a normal rabbit kidney (A) 5 h after excision and (B) 8.5 h after excision.

of the glomeruli, glomerular filtration rate is reduced from 5.9 ± 0.4 to 3.1 ± 0.8 mL/min per kilogram and renal cortical wet/dry weight ratios are increased in association with the edema and inflammation present at this stage. By day 30 widespread scarring is present in both glomeruli and interstitial compartments. This scarring is associated with histologic abnormalities (Masson trichrome-stained scar present in glomeruli and interstitium), increased hydroxyproline concentration (a biochemical measure of scar formation) and decreased renal function depending on the extent of scar formation. Previous studies using this model showed that there is good correlation between the various parameters of scar formation and that hydroxyproline concentration can double without measurable changes in serum creatinine (Downer et al. 1988; McClurkin et al. 1990). Thus, the model reproduces the primary clinical problem, namely the insensitivity of functional measurements to detect scar formation.

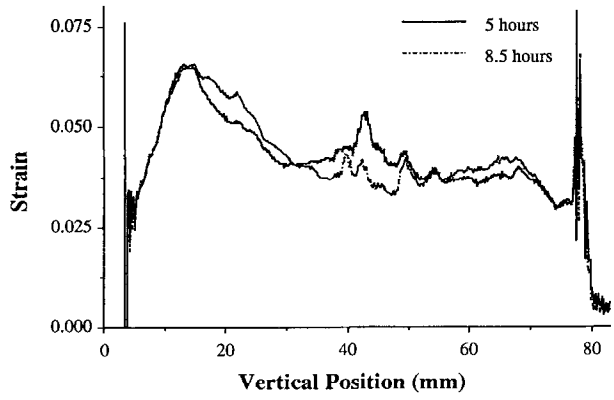

Fig. 5. Strain A-scans along the central vertical line for the phantom with a normal rabbit kidney: (A) 5 h after excision and (B) 8.5 h after excision.

An accelerated model of anti-GBM disease was produced by injecting guinea pig anti-rabbit GBM immunoglobulin into rabbits preimmunized against guinea pig IgG as previously described (Downer et al. 1988). The time course of scarring, distribution of collagen mRNA, T-cell involvement and changes in renal structure and function have been mapped in this model (Downer et al. 1988; McClurkin et al. 1990; Coimbra et al. 1990; Merritt et al. 1990; Holzman and Wiggins 1991; Goyal and Wiggins 1991; Eldredge et al. 1991; Wiggins et al. 1993). This knowledge is key to interpreting kidney elasticity measurements. In the experiments described here, animals were maintained for 120 days after injection to allow inflammation and edema to subside so that any elasticity changes would be attributable to renal scar.

Immediately before excision both kidneys were perfused with normal saline preventing blood coagulation inside the kidney, which may unpredictably affect elasticity measurements. Then, both kidneys were excised from the rabbit and treated separately. One was used for elasticity imaging experiments, *i.e.*, placed in

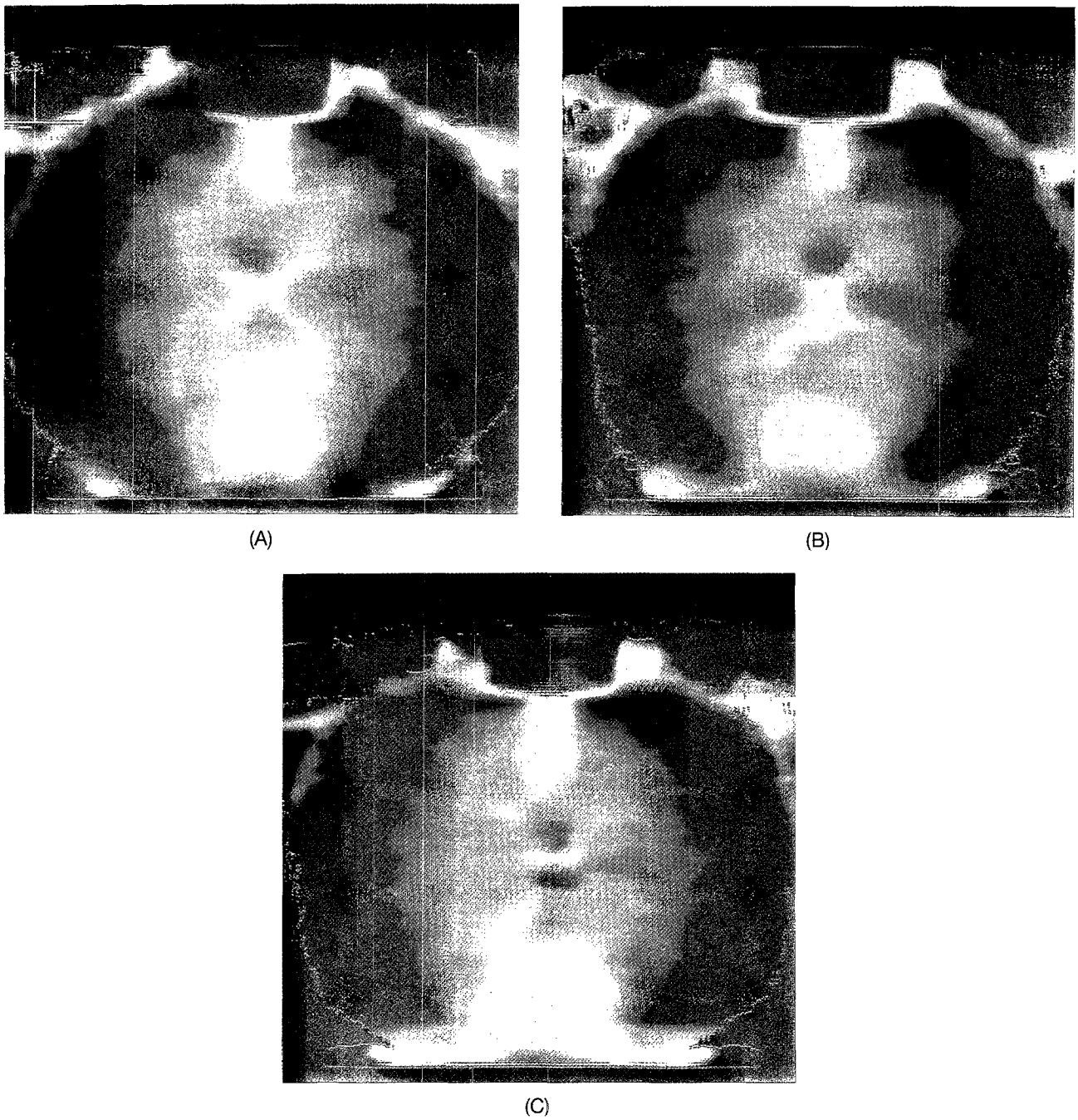

Fig. 6. Images (100 mm by 100 mm) of the vertical, longitudinal component (ϵ_{22}) of the strain tensor for three (A, B, C) different phantoms with a normal rabbit kidney inside.

the gelatin-based phantom described below, and the other was used in control experiments. Following excision, tissue samples were obtained from the control kidney for scar analysis. The renal capsule was removed and the cortex was trimmed off with scissors. A piece of cortex was homogenized in acetic acid, dried in a speed vacuum concentrator and stored at −70°C. Quantitative hydroxyproline concentration was analyzed using the procedure outlined elsewhere (Downer et al. 1988; McClurkin et al. 1990). At the same time, sections for light microscopy were placed in 10% formalin prior to review and histologic scoring. The degree of cortical fibrosis was assessed from Masson's trichrome-stained sections and graded (none, mild, moderate, severe) based on the total amount of blue stain throughout the cortex (sclerosis score) (Downer et al. 1988). The

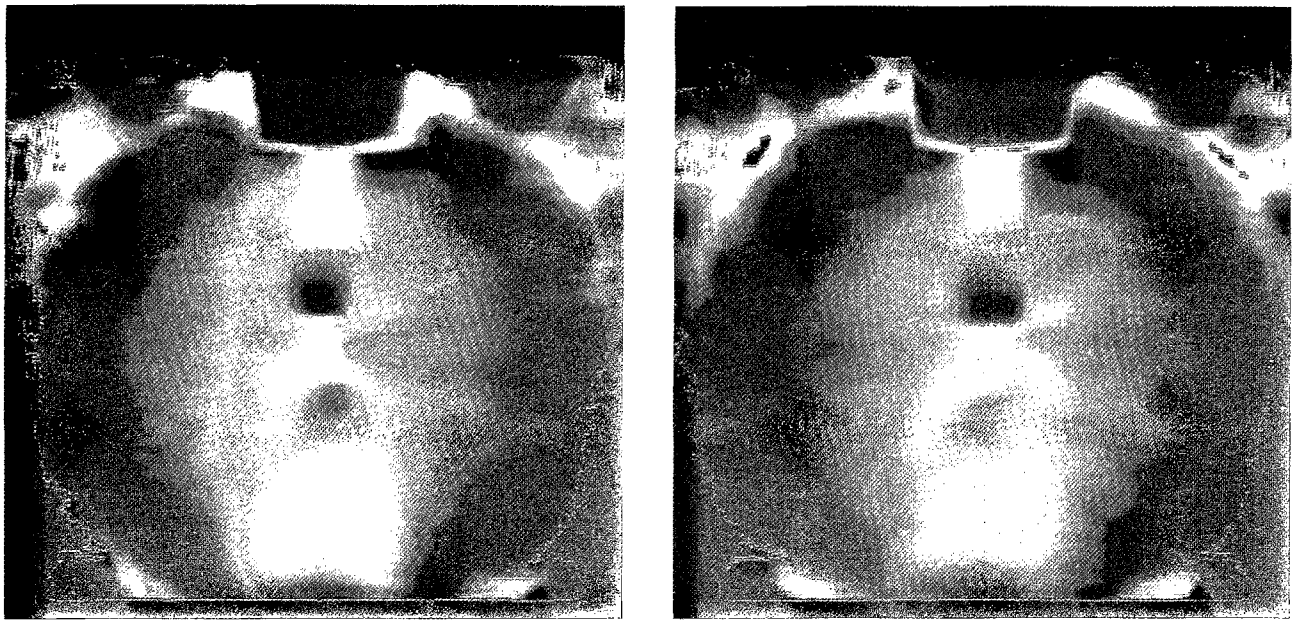

(A) (B)

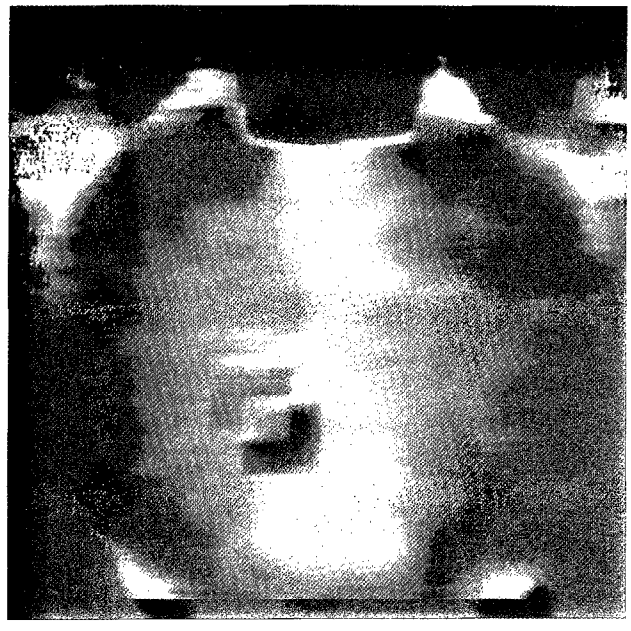

(C)

Fig. 7. Images (100 mm by 100 mm) of the vertical, longitudinal component (ϵ_{22}) of the strain tensor for three (A, B, C) different phantoms with a scarred rabbit kidney inside.

other half of the control kidney was placed in a tube with normal saline. This tube and contents experienced the same time/temperature course as the kidney used in the elasticity experiments. After data acquisition, histologic sections were prepared for both control and elasticity imaged kidneys. These sections were used to assess possible changes in tissue pathology resulting from the experimental procedure.

Strain imaging and experimental procedure

Quantitative strain images were obtained *in vitro*, where the excised goat or rabbit kidney was placed at the center of an otherwise homogeneous gelatin phantom. This is schematically illustrated in Fig. 1. For example, the rabbit kidney cross-section at this position extends about 15 to 20 mm along the transverse plane, similar in orientation to that of a clinical B-scan.

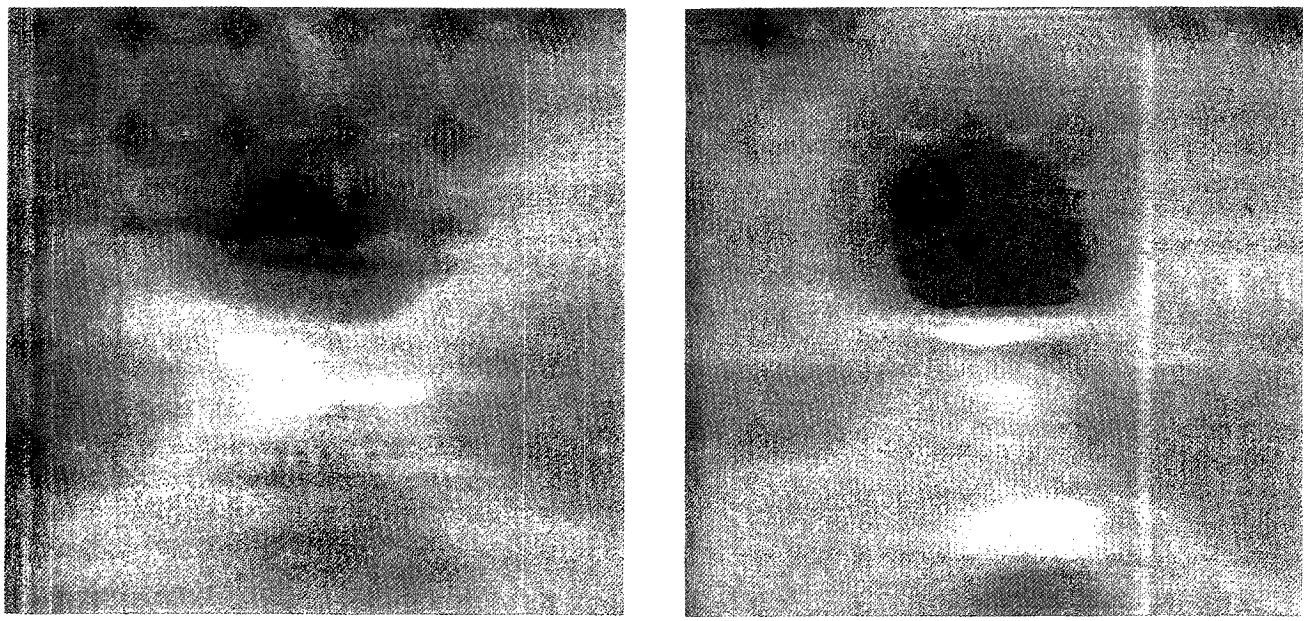

Fig. 8. Magnified (25 mm by 25 mm) images of the vertical, longitudinal component (ϵ_{22}) of the strain tensor for the central part of the phantom: (A) normal kidney and (B) scarred kidney. Phantoms were subjected to 6% average strain.

Thus, the kidney plane analyzed with this preparation closely mimics the clinical environment for both normal kidney and renal transplant.

The gel-based phantoms used here were designed to qualitatively simulate the mechanical properties of soft tissue surrounding the kidney. Methods to fabricate these phantoms and control the Young's modulus are detailed in previous publications (O'Donnell et al. 1994; Skovoroda et al. 1994). Briefly, homogeneous, cylindrical phantoms 88 mm in diameter by 140 mm long, were constructed from 5.5% (by weight) gelatin. A circular longitudinal hole about 25 mm in diameter was then made in the center of the phantom. The excised kidney was placed at the center of this hole and the remainder was backfilled with the same 5.5% (by weight) gelatin. In all phantoms, 0.4% (wt) polystyrene microspheres (diameter of 40 to 120 μm) were added to the gelatin as ultrasonic scattering centers. The scatterer concentration in the backfilled gelatin was the same as in surrounding material.

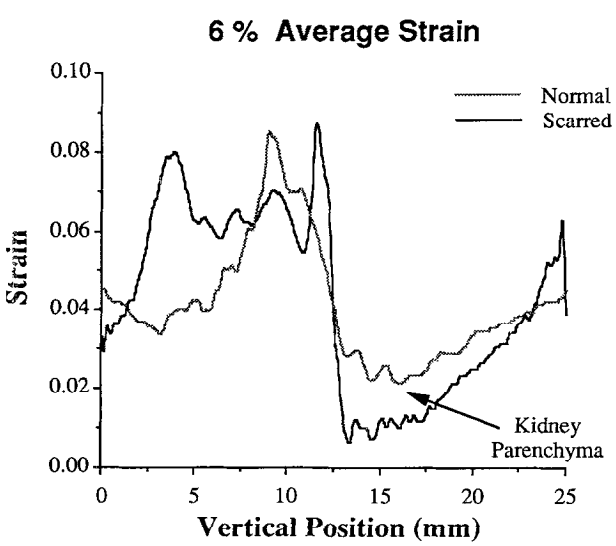

Fig. 9. Strain A-scans along the central vertical line for the phantom with a normal kidney and a scarred kidney. Phantoms were subjected to 6% average strain.

Prior to kidney studies, two homogeneous cylindrical gels were made at the same time with nearly identical mechanical characteristics to test the influence of the backfilled hole itself on strain images. These phantoms again were constructed from 5.5% (wt) gelatin. A circular longitudinal hole about 25 mm in diameter was made in the center of one of the phantoms and then backfilled with the same 5.5% (wt) gelatin. Consequently, the only difference in mechanical properties between these two phantoms must be the result of backfilling.

All phantoms were placed in a water tank with cylindrical axis perpendicular to the axis of a 3.5-MHz, 128-channel, one-dimensional transducer array attached

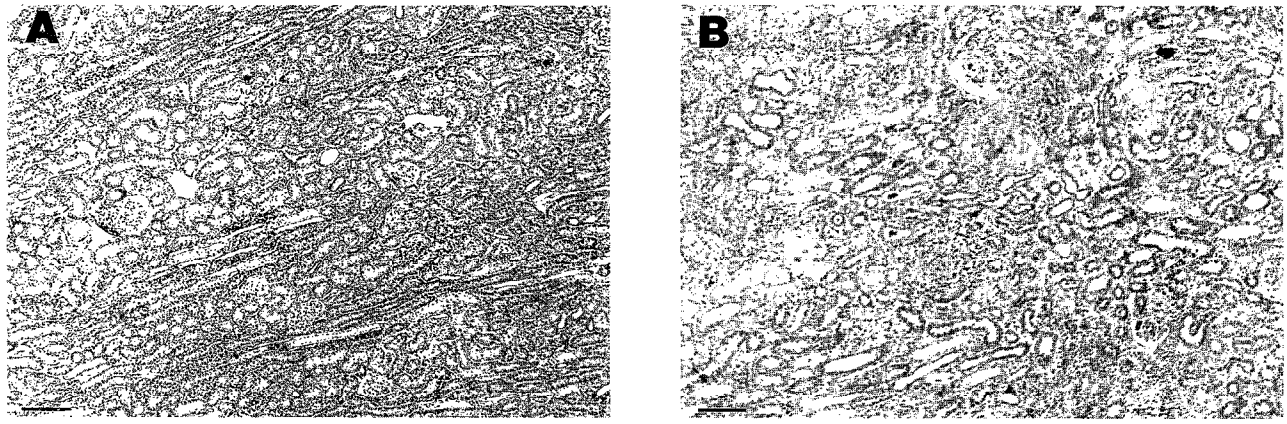

Fig. 10. Photomicrograph of Masson trichrome-stained histological sections: (A) normal rabbit kidney and (B) rabbit kidney with developed scar. These photomicrographs indicate the relatively small damage sustained by the kidney in (B). The bar indicates 200 μm.

to the bottom of the tank, as illustrated in Fig. 1. The phantom was centered so that the image plane approximated the central plane perpendicular to the longitudinal axis of the phantom. The tank was filled with water providing contact between the array and phantom and preventing temperature fluctuation during the experiment. The hydraulically driven pistons shown on the top of the tank were individually connected to 14-mm-wide rigid rectangular blocks extending the entire length of the phantom. As reported previously (O'Donnell et al. 1994; Skovoroda et al. 1994), in the area of the central vertical plane of the phantom, this deformation system closely approximates a plane deformed state. The complete set of pistons can create different complex strain/stress patterns and will be used in the future to develop and test the concept of optimal surface deformation. In the present experiments, however, simple surface displacements were produced only by the vertical piston located at the top of the phantom, where movement of this piston was controlled by measuring ultrasonic pulse arrival time differences to central array elements.

The strain imaging method has been previously reported (O'Donnell et al. 1994). In particular, complex baseband images were reconstructed using a modified synthetic aperture approach, where special processing was included in image reconstruction to minimize grating lobes produced by the large array elements (approximately 1.5 acoustic wavelength spacing). Because traditional speckle tracking techniques fail in the limit of very large motion, a method of properly accumulating small displacements was used to track internal motion due to significant (*i.e.*, on the order of many acoustic wavelengths) surface displacement (O'Donnell et al. 1994). Using a large set of baseband images acquired during surface deformation, where consecutive measurements within each set were separated by a piston displacement of either 200 or 300 μm, both displacement and strain images were reconstructed with average internal strain ranging from 5% to 15%. The average strain is defined here as the percent change in the vertical size of the phantom before and after deformation. Note that the strain magnitude at some regions may exceed the average strain due to tissue elasticity variations, boundary conditions, *etc.* (O'Donnell et al. 1994, Skovoroda et al. 1994).

The period between rabbit kidney excision and the beginning of data acquisition was approximately 4 h.

Table 1. Comparison of functional, biochemical and histologic studies on normal and scarred rabbit kidneys.

Animal	Corresponding figure	Hydroxyproline (mg/g dry weight)	Hydroxyproline (mg/g wet weight)	Serum creatinine (mg/100 mL)	Histology: Interstitial fibrosis	Histology: % Scarred glomerili
Normal 1	Fig. 7A	4.75	0.798	1.0	None	0.0
Normal 2	Fig. 7B	3.59	0.652	1.1	None	0.6
Scarred 1	Fig. 8A	9.73	1.662	1.4	Mild patchy	16.4
Scarred 2	Fig. 8B	4.45	0.735	1.2	Mild patchy	13.9
Scarred 3	Fig. 8C	6.62	1.176	1.0	Mild patchy	2.8

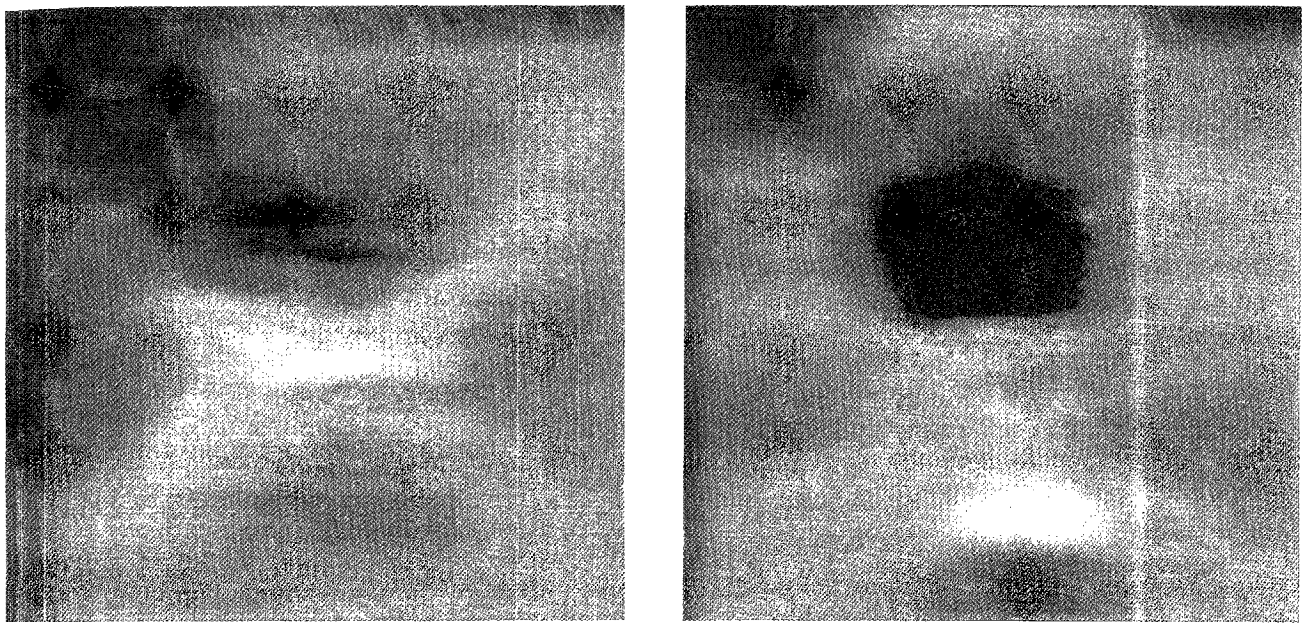

(A) (B)

Fig. 11. Magnified (25 mm by 25 mm) images of the vertical, longitudinal component (ϵ_{22}) of the strain tensor for the central part of the phantom: (A) normal kidney and (B) scarred kidney. Phantoms were subjected to 11% average strain.

Most of this time was needed to stabilize temperature between the phantom, kidney and coupling water in the tank since the elasticity of both tissue and gel is highly dependent on temperature (Abbott and Steiger 1977). The large amount of water in the tank, however, helped to reduce temperature fluctuations during the experiment. All experiments were performed at a temperature of 20 ± 1°C as determined by the thermometer shown in Fig. 1.

Finally, all of the experiments in this study can be summarized into two subsequent groups: control studies and rabbit kidney studies. The first group was designed to validate the experimental protocol. It consisted of experiments with two homogeneous phantoms constructed to test the influence of the backfilled hole; experiments with an excised normal goat kidney and a goat kidney with artificially created "lesions" to test the ability of strain imaging in highly inhomogeneous tissues; and studies on normal rabbit kidneys to test the effect of various experimental conditions on strain images. The second group of experiments was designed to test the hypothesis that elasticity imaging can detect renal pathology. Only normal rabbit kidneys and kidneys excised from rabbits with experimental anti-GBM disease were used in this group. Strain images of normal and scarred rabbit kidneys were contrasted and compared with the results of biochemical, functional and histologic analysis.

RESULTS

Control studies

Control experiments were first performed on the pair of nearly identical homogeneous phantoms constructed to test the influence of the backfilled hole. Vertical, longitudinal strain (ϵ_{22}) images from these two phantoms displayed over a 100-mm by 100-mm area are shown in Fig. 2, where the transducer is on the bottom and the central piston is on the top. The strain distribution in the homogeneous noncomposite phantom (Fig. 2A) is contrasted with that in the homogeneous composite phantom with a backfilled hole in the center (Fig. 2B). Bright areas in these images, and all subsequent strain images, correspond to regions of high strain. Both images in Fig. 2 are displayed over the same dynamic range of 0.082 to 0.188, *i.e.,* full brightness represents a longitudinal strain of 18.8% and complete darkness represents a strain of 8.2%. Note that these strain images were computed for a 13.2-mm displacement of the piston (*i.e.,* 15% average strain) and were scaled to the full strain dynamic range of 30%, since the strain magnitude at some points may exceed the average strain due to various factors such as the elasticity distribution, boundary conditions, *etc.* Clearly, the backfilled hole does not create large artifacts. Similar results were obtained for lower average strain, *i.e.,* for smaller displacement of the piston.

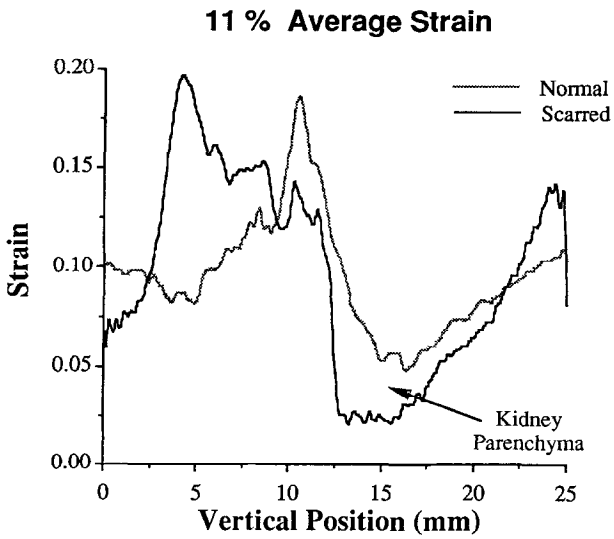

Fig. 12. Strain A-scans along the central vertical line for the phantom with a normal kidney and a scarred kidney. Phantoms were subjected to 11% average strain.

Strain images of two excised goat kidneys are contrasted in Fig. 3, where a 50-mm by 50-mm region, including the entire kidney, is presented with a display dynamic range of 0.006 to 0.171, *i.e.*, 0.6% to 17.1% strain. Again, the full dynamic range for these images is 30%. The kidney imaged in Fig. 3A was directly excised whereas the kidney imaged in Fig. 3B was injected with the crosslinking agent at two sites within it prior to excision. The hard "lesions" are clearly visible in Fig. 3B as dark low strain regions. Although these images are quite complex, changes in tissue elasticity are easily detectable with strain images even in a highly inhomogeneous medium such as the kidney.

Results of control studies on normal rabbit kidneys are presented in Figs. 4 and 5. Figure 4 contrasts strain images of a normal rabbit kidney obtained at two different times following excision. Fig. 4A was acquired 5 h after excision and Fig. 4B was acquired 8.5 h after excision. These images represent a 100-mm by 100-mm region. Bright areas correspond to regions with higher strain. The display dynamic range is 0.014 to 0.053 generated with an average strain of about 6%. Clearly, there are no major differences in these images. A more quantitative comparison is presented in Fig. 5, where strain A-scans along the central vertical line for these two images are shown. Contrasted to the types of differences expected from renal scar, little change is observed in strain data as a function of time after excision. Histologic sections taken at various times following excision showed no major histologic changes. A small degree of vacuolation in renal tubular cells was noted in both experimental and control kidneys which was probably related to the time the organ had been removed from the rabbit. These changes were considered not significant, and consistent with the small changes in strain evident in Figs. 4 and 5. Additional data taken at times between 5 and 8.5 h after excision also showed little change.

Rabbit kidney studies

First, studies were conducted to assess variability in strain images of normal rabbit kidneys. Results of this study, presented in Fig. 6, contrast strain images of normal kidneys excised from three different rabbits. These 6% average strain images are displayed over a 100-mm by 100-mm region with a dynamic range of 0.015 to 0.055. Although differences are evident, reduction in strain due to renal scar (*i.e.*, tissue hardening) far exceeds strain variability in normal kidney parenchyma, as shown below. Consequently, results on normal rabbit kidneys, presented in Fig. 6, suggest that the present protocol can critically test the hypothesis that changes in elasticity due to scarring are detectable using quantitative strain imaging.

Strain images of three scarred kidneys are presented in Fig. 7 for a 6% average strain, where the same display dynamic range as normal kidneys (Fig. 6) was used. These diseased kidneys were excised at approximately 120 days after injecting anti-GBM antibodies, a period selected to ensure full scar development including collagen crosslinking. Note that the kidney in Fig. 7C was accidentally offset from the center of the phantom. As evident from these images, lower strain is obtained in scarred kidney parenchyma signaling a significantly increased elastic modulus (*i.e.*, hardness). Reduction in strain within kidney parenchyma is more pronounced in Fig. 7 compared to either Fig. 4 or Fig. 6. Further demonstration of this is given in Fig. 8, where a four-times-magnified image (*i.e.*, a 25-mm by 25-mm central region) of one of the normal kidneys (Fig. 8A) is contrasted with that of one of the scarred kidneys (Fig. 8B). Central vertical A-scans through both these images are presented in Fig. 9, where 0 mm corresponds to the bottom of the image and 25 mm to the top, and regions of kidney parenchyma are noted.

Masson trichrome-stained histological sections taken from these same two kidneys immediately following excision are compared in Fig. 10. Although histologic sections taken from the kidney after the experiment show slight vacuolations due to time (approximately 5 h) and temperature changes, differences due to scarring shown in Fig. 10 are unaltered by the experimental procedure. Widespread mild fibrosis is evident in the scarred kidney section (Fig. 10B) compared

to the normal kidney (Fig. 10A). Serum creatinine concentration changes, however, are still minor.

The results of functional, biochemical and histologic studies on all rabbits are summarized in Table 1. Clear regions of mild, patchy scar were evident although renal function, as measured by serum creatinine, was minimally abnormal in only one animal. Scarred kidneys showed enhanced collagen concentration, where the hydroxyproline concentration compared to the average of the two normal kidneys was enhanced by factors of 1.6 and 2.3 in two cases and just slightly increased in the other case. The kidney with most pronounced changes in hydroxyproline concentration, most scarring by histology and a slightly increased serum creatinine of 1.4 mg per 100 mL (normal for rabbits ranges between 0.8 and 1.25 mg per 100 mL) also exhibited the largest reduction in strain (Fig. 7A).

All experimental results on rabbit kidneys presented above were obtained with average strains of about 6%, *i.e.*, 5-mm vertical displacement of the central piston. As a further test of the large strain imaging method described in O'Donnell et al. (1994), a number of experiments were performed at much higher average strains. Four-times-magnified (*i.e.*, 25 mm by 25 mm) strain images of the same kidneys as in Fig. 8, but at an average strain of 11%, are presented in Fig. 11. The strain signal-to-noise ratio (SNR) in these images is about two times better than in their smaller strain counterparts. Further demonstration of this is shown in Fig. 12, where the central vertical strain A-scans for these images are compared. Even though linear elasticity may be violated at these high strain levels, the results in Figs. 11 and 12 show that greatly increased strain SNR can be produced with large average strains even in highly inhomogeneous organs such as the kidney.

DISCUSSION

Preliminary results reported in this study show that precise measures of the strain distribution are possible even in highly inhomogeneous organs such as the kidney. This was demonstrated for the goat kidney model (Fig. 3) where two artificial "lesions" created within the organ are clearly visible. In addition, changes in kidney elasticity indicative of renal scar in an animal model of nephritis were easily detected using large average strain. Obviously, the small set of results shown in Figs. 6 and 7 for the rabbit model of chronic nephritis does not prove a direct correlation between renal scar and increased elastic modulus. These images do, however, suggest that scar can be detected by quantitative strain imaging. Moreover, these results strongly suggest that mild-to-moderate scarring can be detected prior to major changes in kidney function.

The relation between changes in elastic Young's modulus, scar formation and histologic, functional and biochemical indexes is not simple. All three scarred kidneys studied here showed mild scarring easily detected by histology, but only two exhibited an abnormal increase in collagen concentration as presented in Table 1. Nevertheless, all scarred kidneys showed a decrease in strain magnitude in the area of the cortex signaling an increase in the Young's modulus. It is possible that the elasticity of scarred tissue is dependent not only on the concentration of collagen but also on its state, such as fully developed crosslinking. In the present study, diseased kidneys were excised at approximately 120 days after injecting anti-GBM antibodies. This period ensured both full scar development and collagen crosslinking and may explain why one of the diseased kidneys exhibited strain reduction even though collagen concentration was only slightly elevated. Future work must be done to investigate this phenomenon. One possible way to identify the relation between the concentration and state of collagen and related elasticity changes will be direct independent measurements of the elastic (Young's) modulus. These measurements can be achieved, for example, with an invasive contact method using small tissue samples (Sarvazyan et al. 1993).

Strain imaging does not solely depend on tissue elasticity and, in general, also depends on the boundary conditions, types of external loads, the geometry of the imaged object, *etc.* (O'Donnell et al. 1994; Skovoroda et al. 1994; Emelianov et al. 1995). Therefore, robust reconstruction methods converting geometry-dependent strain images to images of the elasticity distribution must be developed to remove strain imaging artifacts (Emelianov et al. 1995). This is not important, for example, for a one-dimensional model, where the geometry is simple. More complicated strain images are obtained in two- and three-dimensional cases for complex surface deformations. Clearly, neither simple one-dimensional deformations, or even the present orientation of the transducer and piston used in this study, will be possible in clinical practice with limited ultrasound access to the kidney. However, the strain imaging method used here is in no way restricted to the particular geometry of Fig. 1 (O'Donnell et al. 1994). These and other important clinical concerns, such as the time required for complete data acquisition (O'Donnell et al. 1994), will be investigated in future studies.

Finally, the primary contrast mechanism in elasticity imaging is the Young's modulus of soft tissue. This physical constant is not directly employed in any other modality including NMR, x-ray computed tomography (CT) and ultrasound imaging systems.

Therefore, elasticity imaging represents a new modality even if conventional imaging systems are used to assess motion. The ultimate quality of elasticity images derived from tracking studies is determined by the accuracy of measured strains and displacements (Emelianov et al. 1995). As demonstrated in Figs. 11 and 12, strain images obtained with large surface deformations exhibit much higher SNR compared to those generated with traditional methods. Indeed, the SNR in these images is between one and two orders of magnitude greater than previously published tissue studies (Ophir et al. 1991; Ponnekanti et al. 1992). Using such high SNR displacement and strain images, successful reconstruction methods have recently been shown for simple phantom studies (O'Donnell et al. 1993; Emelianov et al. 1995). Future work will be directed toward expanding these methods to handle complex structures such as the kidney.

Acknowledgements—Partial support from the National Institutes of Health under Grants CA 54896 and DK 47324, General Electric, Acuson and the Office of Vice President for Research at the University of Michigan are gratefully acknowledged. Also, we would like to thank M. Goyal (Department of Internal Medicine, University of Michigan) for help with kidney preparations used in these studies and Dr. S. Phan (Department of Pathology, University of Michigan) for performing the hydroxyproline measurements. M. A. Lubinski was supported under a National Science Foundation Graduate Research Fellowship.

REFERENCES

Abbott, R. H.; Steiger, G. J. Temperature and amplitude dependence of tension transients in glycerinated skeletal and insect fibrillar muscle. J. Physiol. 266:13–42; 1977.

Adler, R. S.; Rubin, J. M.; Bland, P. H.; Carson, P. L. Characterization of transmitted motion in fetal lung: Quantitative analysis. Med. Phys. 16:333–337; 1989.

Adler, R. S.; Rubin, J. M.; Bland, P. H.; Carson, P. L. Quantitative tissue motion analysis of digitized M-mode images: Gestational differences of fetal lung. Ultrasound Med. Biol. 16:561–569; 1990.

Axel, L.; Dougherty, L. Heart wall motion: Improved method of spatial modulation of magnetization for MR imaging. Radiology 169:59–63; 1988.

Bertrand, M.; Meunier, J.; Doucet, M.; Ferland, G. Ultrasonic biomechanical strain gauge based on speckle tracing. Proc. 1989 IEEE Ultrasonics Symp. 2:859–864; 1989.

Chapman, J. R.; Allen, R. D. Dialysis and transplantation. In: Morris, P. J., ed. Kidney transplantation principles and practice. Philadelphia: Saunders; 1988:37–69.

Chen, E. J.; Jenkins, W. K.; O'Brien, W. D. The accuracy and precision of estimating tissue displacement from ultrasonic images. Proc. 1992 IEEE Ultrasonics Symp. 2:1061–1064; 1992.

Coimbra, T. M.; Wiggins, R. C.; Noh, J. W.; Merritt, S. E.; Phan, S. H. Transforming growth factor-b production in anti-glomerular basement disease in the rabbit. Am. J. Pathol. 138:223–234; 1990.

Dickinson, R. J.; Hill, C. R. Measurement of soft tissue motion using correlation between A-scans. Ultrasound Med. Biol. 8:263–271; 1982.

Downer, G.; Phan, S.; Wiggins, R. Analysis of renal fibrosis in a rabbit model of crescentic nephritis. J. Clin. Invest. 82:998–1005; 1988.

Dunnill, M. S. Histopathology of rejection in renal transplantation. In: Morris, P. J., ed. Kidney transplantation principles and practice. Philadelphia: Saunders, 1988:439–472.

Eisensher, A.; Schweg-Toffler, E.; Pelletier, G.; Jacquemard, G. La palpation echographique rythmee—Echosismographie. Journal de Radiologie 64:225–261; 1983.

Eldredge, C.; Merritt, S.; Goyal, M.; Kulaga, H.; Kindt, T. J.; Wiggins, R. Analysis of T cells and MHC Class I and Class II mRNA and protein content and distribution in anti-GBM disease in the rabbit. Am. J. Pathol. 139:1021–1035; 1991.

Emelianov, S. Y.; Skovoroda, A. R.; Lubinski, M. A.; O'Donnell, M. Reconstructive elasticity imaging. In: Jones, J. P., ed. Acoustical imaging 21. New York: Plenum Press; 1995:241–252.

Fowlkes, J. B.; Yemelyanov, S. Y.; Pipe, J. G.; Carson, P. L.; Adler, R. S.; Sarvazyan, A. P.; Skovoroda, A. R. Possibility of cancer detection by means of measurement of elastic properties. Radiology 185:206–207; 1992.

Goyal, M.; Wiggins, R. Fibronectin mRNA and protein accumulation, distribution and breakdown in rabbit anti-GBM disease. J. Am. Soc. Nephrol. 1:1334–1342; 1991.

Harris, R. C.; Meyer, T. W.; Brenner, B. M. Nephron adaptations to renal injury. In: Brenner, B.; Rector, F. C., eds. The kidney. Philadelphia: Saunders; 1986:1553–1586.

Holzman, L. B.; Wiggins, R. C. Glomerular crescent formation. Sem. Nephrol. 11:346–353; 1991.

Ishihara, K.; Tanouchi, J.; Kitabatake, A.; Uematsu, M.; Masuyma, T.; Yoshida, Y.; Doi, Y.; Kondo, H.; Kamada, T.; Kishimoto, S.; Ogawa, T.; Yokozawa, N.; Mulai, H.; Kodama, M. High speed digital subtraction echography: Principle and preliminary application to arteriosclerosis, arythmia and blood flow visualization. Proc. 1990 IEEE Ultrasonics Symp. 2:1473–1476; 1990.

Krouskop, T. A.; Dougherty, D. R.; Levinson, S. F. A pulsed Doppler ultrasonic system for making non-invasive measurements of the mechanical properties of soft tissue. J. Rehabil. Res. Dev. 24:1–8; 1987.

Lee, F.; Bronson, J. P.; Lerner, R. M.; Parker, K. J.; Huang, S. R.; Roach, D. J. Sonoelasticity imaging: results in *in vitro* tissue specimens. Radiology 181:237–239; 1991.

Lerner, R. M.; Parker, K. J.; Holen, J.; Gramiak, R.; Waag, R. C. Sono-elasticity: Medical elasticity images derived from ultrasound signals in mechanically vibrated targets. In: Acoustical imaging 16. New York: Plenum Press; 1988:317–327.

Lerner, R. M.; Huang, S. R.; Parker, K. J. "Sonoelasticity" images derived from ultrasound signals in mechanically vibrated tissues. Ultrasound Med. Biol. 16:231–239; 1990.

Lerner, R. M.; Parker, K. J. Sono-elasticity in ultrasonic tissue characterization and echo-graphic imaging. In: Thijssen, J. M., ed. Proceedings of the 7th European Communities Workshop, Nijmegen; 1987.

McClurkin, C., Jr.; Phan, S. H.; Hsu, C. H.; Patel, S. R.; Spicker, J. K.; Kshirsagar, A. M.; Yuan, W.; Wiggins, R. C. Moderate protection of renal function and reduction of fibrosis by colchicine in a model of anti-GBM disease in the rabbit. J. Am. Soc. Nephrol. 1:257–265; 1990.

Merritt, S. E.; Killen, P. D.; Phan, S. H.; Wiggins, R. C. Analysis of a1 (I) procollagen, a1 (IV) collagen and b-actin mRNA in glomerulus and cortex of rabbits with experimental anti-GBM disease. Evidence for early extraglomerular collagen biosynthesis. Lab. Invest. 63:762–769; 1990.

Meunier, J.; Bertrand, M. Ultrasonic speckle motion inherent to tissue motion: Theory and simulation. Proc. 1989 IEEE Ultrasonics Symp. 2:865–868; 1989.

O'Donnell, M.; Skovoroda, A. R.; Shapo, B. M. Measurement of arterial wall motion using Fourier based speckle tracking algorithms. Proc. 1991 IEEE Ultrasonics Symp. 2:1101–1104; 1991.

O'Donnell, M.; Emelianov, S. Y.; Skovoroda, A. R.; Lubinski, M. A.; Weitzel, W. F.; Wiggins, R. C. Quantitative elasticity imaging. Proc. 1993 IEEE Ultrasonics Symp. 2:893–903; 1993.

O'Donnell, M.; Skovoroda, A. R.; Shapo, B. M.; Emelianov, S. Y. Internal displacement and strain imaging using ultrasonic speckle tracking. IEEE Trans. Ultrasonic Ferroelec. Freq. Control 41:314–325; 1994.

Ophir, J.; Cespedes, I.; Ponnekanti, H.; Yazdi, Y.; Li, X. Elastogra-

phy: A quantitative method for imaging the elasticity of biological tissues. Ultrason. Imag. 13:111–134; 1991.

Parker, K. J.; Huang, S. R.; Musulin, R. A.; Lerner, R. M. Tissue response to mechanical vibrations for "sonoelasticity imaging." Ultrasound Med. Biol. 16:241–246; 1990.

Parker, K. J.; Lerner, R. M. Sonoelasticity of organs: Shear waves ring a bell. J. Ultrasound Med. 11:387–392; 1992.

Ponnekanti, H.; Ophir, J.; Cespedes, I. Axial stress distributions compressors in elastography: An analytical model. Ultrasound Med. Biol. 18:667–673; 1992.

Ryan, L. K.; Lockwood, G. R.; Starkoski, B. G.; Holdsworth, D. W.; Rickey, D. W.; Drangova, M.; Fenster, A.; Foster, F. S. A high frequency intravascular imaging system for investigation of vessel wall properties. Proc. 1992 IEEE Ultrasonics Symp. 2:1101–1105; 1992.

Sarvazyan, A.; Maevsky, E.; Gukassian, D.; Skovoroda, A.; Emelianov, S.; Berzhanskaja, Y.; Oranskaja, G.; Klishko, A. On the diagnostic value of ultrasound elasticity imaging of the breast. Abstract of the 1993 IEEE Ultrasonics Symposium; 1993.

Sarvazyan, A. P.; Skovoroda, A. R. The new approaches in ultrasonic visualization of cancers and their qualitative mechanical characterization for the differential diagnostics. In: The actual problems of the cancer ultrasonic diagnostics. Moscow; 1990.

Sarvazyan, A. P.; Skovoroda, A. R. Tissue characterization in medical imaging in terms of viscoelastic mechanical properties. Abstract of 6th World Congress on Ultrasound, Copenhagen; 1991.

Skovoroda, A. R.; Emelianov, S. Y.; Lubinski, M. A.; Sarvazyan, A. P.; O'Donnell, M. Theoretical analysis and verification of ultrasound displacement and strain imaging. IEEE Trans. Ultrason. Ferroelec. Freq. Control 41:302–313; 1994.

Tristam, M.; Barbosa, D. C.; Cosgrove, D. O.; Nassiri, D. K.; Bamber, J. C.; Hill, C. R. Ultrasonic study of *in vivo* kinetic characteristics of human tissue. Ultrasound Med. Biol. 12:927–937; 1986.

Tristam, M.; Barbosa, D. C.; Cosgrove, D. O.; Bamber, J. C.; Hill, C. R. Application of fourier analysis to clinical study of patterns of tissue movement. Ultrasound Med. Biol. 14:695–707; 1988.

Wiggins, R.; Goyal, M.; Merritt, S.; Killen, P. D. Vascular adventitial cell expression of collagen I mRNA in anti-GBM antibody-induced crescentic nephritis in the rabbit. A cellular source for interstitial collagen synthesis in inflammatory renal disease. Lab. Invest. 68:557–565; 1993.

Yamakoshi, Y.; Sato, J.; Sato, T. Ultrasonic imaging of the internal vibration of soft tissue under forced vibration. IEEE Trans. Ultrason. Ferroelec. Freq. Control 37:45–53; 1990.

Yamashita, Y.; Kubota, M. Tissue characterization from ultrasonic imaging of movement and deformation. Proc. 1990 IEEE Ultrason. Symp. 2:1371–1375; 1990.

Yemelyanov, S. Y.; Skovoroda, A. R.; Lubinski, M. A.; Shapo, B. M.; O'Donnell, M. Ultrasound elasticity imaging using Fourier based speckle tracking algorithm. Proc. 1992 IEEE Ultrason. Symp. 2:1065–1068; 1992.

Zerhouni, E. A.; Parish, D. M.; Rogers, W. J.; Yang, A.; Shapiro, E. P. Human heart: Tagging with MR imaging—a method for noninvasive assessment of myocardial motion. Radiology 169:164–172; 1988.